Eur. Phys. J. C 6, 35–41 (1999)
DOI 10.1007/s100529801012

THE EUROPEAN PHYSICAL JOURNAL C

A measurement of the form-factor ratios in the decay $D^+ \to \bar{K}^{*0}\mu^+\nu_\mu$

The BEATRICE Collaboration

M. Adamovich[5], Y. Alexandrov[5], C. Angelini[6], D. Barberis[3], F. Ceradini[8], C. Cianfarani[1], M. Dameri[3], G. Darbo[3], A. Duane[4], V. Flaminio[6], A. Forino[1], B.R. French[2], A. Frenkel[7], C. Gemme[3], K. Harrison[7], N. Hummadi[4], R. Hurst[3], A. Kirk[2], C. Lazzeroni[6], L. Malferrari[1], G. Martellotti[7], P. Martinengo[2], P. Mazzanti[1], J.G. McEwen[9], P. Nechaeva[5], B. Osculati[3], M. Passaseo[7], G. Penso[7], A. Quareni[1], L. Rossi[3], M. Verzocchi[7], D. Websdale[4], M. Zavertyaev[5]

[1] Università di Bologna and INFN, Bologna, Italy
[2] CERN, Geneva, Switzerland
[3] Università di Genova and INFN, Genoa, Italy
[4] Blackett Laboratory, Imperial College, London, UK
[5] Lebedev Physical Institute, Moscow, Russian Federation
[6] Università di Pisa and INFN, Pisa, Italy
[7] Università di Roma "La Sapienza" and INFN, Rome, Italy
[8] Università di Roma "Roma Tre" and INFN, Rome, Italy
[9] University of Southampton, Southampton, UK

Received: 10 July 1998 / Revised version: 10 August 1998 / Published online: 19 October 1998

Abstract. The form-factor ratios in the decay $D^+ \to \bar{K}^{*0}\mu^+\nu_\mu$ have been measured using a sample of 763 events produced in the WA92 fixed-target experiment. The values obtained are $R_V = 1.45 \pm 0.23 \pm 0.07, R_2 = 1.00 \pm 0.15 \pm 0.03$ and the corresponding ratio of longitudinal to transverse polarisation is $\Gamma_L/\Gamma_T = 1.09 \pm 0.10 \pm 0.02$.

1 Introduction

The Standard Model describes the semileptonic decay of hadrons as the product of a well-understood leptonic current and a hadronic current. The latter describes the evolution from the initial- to the final-state hadron and involves strong-interaction corrections to the weak current. The basic couplings between the quarks that contribute to the hadronic current are parameterised by the CKM quark-mixing matrix. Most of the known matrix elements have been measured using semileptonic decays, a procedure that requires theoretical calculations of the form factors describing how the strong interactions modify the underlying weak process.

Semileptonic B decays to charmed final states have been used to measure the magnitude of V_{cb}. In these decays both initial- and final-state hadrons contain one heavy quark ($m_Q \gg \Lambda_{QCD}$) and one light quark. This permits the use of heavy-quark effective theory (HQET), which, in this approximation, derives directly from QCD. The same approximations do not apply in semileptonic B decays to non-charmed final states. The extraction of V_{ub} from the data therefore requires alternative theoretical input, for which several quark-model calculations have been performed.

In contrast to V_{cb} and V_{ub}, the elements V_{cs} and V_{cd} can be determined from the unitarity constraints of the CKM matrix. The experimental measurement of the form factors in semileptonic decays of charmed particles permits a comparison of data with the predictions of the quark models, thus providing a check on the model dependence of the V_{ub} measurement from semileptonic B decay. The theoretical and experimental status of this subject has been reviewed by Richman and Burchat [1].

We present an analysis of the angular distribution of the decay

$$D^+ \to \bar{K}^{*0}\mu^+\nu_\mu \to K^-\pi^+\mu^+\nu_\mu,$$

and its charge-conjugate, using a sample of 763 events produced by interactions of $350\,\mathrm{GeV}/c$ π^- on a fixed target in experiment WA92 at the CERN SPS.

In analysing the decay, we follow the method adopted by E653 [2] and E687 [3] and use the quark model of Körner and Schuler [4] who calculate the decay rate without assuming a zero-mass lepton. Wirbel, Stech and Bauer [5] give the decay matrix element in terms of one vector (V), two axialvector (A_1, A_2) and one pseudoscalar (A_0) form factors:

$$\langle K^*|j_\mu|D\rangle = 2\varepsilon_{\mu\nu\rho\sigma}\epsilon^{*\nu}\,P_D^\rho P_{K^*}^\sigma V(q^2)/(m_D + m_{K^*}) + i\{\epsilon_\mu^*\,(m_D + m_{K^*})A_1(q^2)$$

$$-\epsilon^* \cdot q\,(P_D + P_{K^*})_\mu A_2(q^2)/(m_D + m_{K^*})$$
$$-2\epsilon^* \cdot q\, m_{K^*} q_\mu A_3(q^2)/q^2\}$$
$$+2i\epsilon^* \cdot q\, m_{K^*} q_\mu A_0(q^2)/q^2\ ,$$

where $A_3(q^2) = (m_D + m_{K^*})A_1(q^2)/2m_{K^*}$
$-(m_D - m_{K^*})A_2(q^2)/2m_{K^*}$,
ϵ^* is the K^* polarisation vector and $q_\mu = (P_D - P_{K^*})_\mu$ is the difference of the D and K^* 4-momenta. Since we do not measure the absolute decay rate, we use our measurement of the experimental decay distributions to extract the following ratios of vector and axial-vector form factors; $R_V = V(0)/A_1(0)$ and $R_2 = A_2(0)/A_1(0)$.

2 Experiment

The apparatus was mounted in the Ω' spectrometer [6] and is described in [7]. Copper and tungsten targets (2 mm thick) were used. The spectrometer contained multiwire proportional chambers, drift chambers and silicon tracking, which give angular precision at the vertex of ≈ 0.2 mrad and momentum precision of $\sigma_p/p^2 = 1.5 - 3.0 \times 10^{-4}\,(\mathrm{GeV}/c)^{-1}$. The silicon tracking planes were in four groups. A beam telescope reconstructed the coordinates of the incident particle at the target, with 5 μm standard deviation transverse to the beam. A single plane attached to the exit face of the target was used in the trigger to suppress interactions occurring outside the target. In the region $2 - 32$ mm downstream of the target, the Decay Detector (DkD), a group of 17 planes with 10 μm pitch and analogue readout of pulse height, contained most of the charm decay vertices. In the region $66 - 630$ mm downstream of the target, the Vertex Detector (VxD), a group of 17 planes of 25 or 50 μm pitch with binary readout, was used in the trigger to detect tracks offset from the primary vertex. Information from all four groups was recorded for the analysis. A hodoscope of two layers of scintillator slabs, shaped to be insensitive to particles with $p_T < 0.6\,\mathrm{GeV}/c$, was placed at the exit of the magnet. This was followed by an electromagnetic calorimeter, 22 radiation lengths thick (not used in this analysis). Muons were detected by a group of resistive-plate chambers (RPC) placed downstream of 2 m of iron, and a second group placed downstream of a further 1.2 m of iron. There was no identification of kaons.

Data were recorded over 110 days of beam time during 1992 and 1993 with an integrated luminosity of 1.5 nb^{-1} on tungsten, 8.1 nb^{-1} on copper. The trigger accepted 2 MUON or MUON·IP(2) or MUON·P_T (in 1992) or MUON·IP(1) (in 1993) where

i) IP(n) was true if at least 3 tracks were found in VxD with impact parameter to the primary vertex ip $<$ 100 μm and at least n tracks were found with 100 μm $<$ ip $<$ 1000 μm,
ii) P_T was true if a track was detected by a coincidence between the two p_T hodoscope planes and
iii) MUON was true if a track was detected in the RPC with direction emanating from the target.

Simulated events were generated using PYTHIA [8] for the production of $c\bar{c}$ and JETSET 7.3 [9] for their fragmentation. This used less than the full energy of an event. The remaining energy was used by FLUKA [10] to generate a π^--nucleus interaction. All interaction products were tracked through the apparatus using GEANT 3.21 [11]. This is described more fully in [7].

3 Event selection

After reconstruction of charged tracks and vertices, semileptonic decays were required to have:

i) a primary vertex in the target,
ii) a secondary three-prong vertex separated by $\geq 30\,\sigma$ (≈ 6 mm) from the primary and inside a fiducial region between 2 mm and 61 mm downstream of the target centre,
iii) no energy deposit large enough to signal an interaction in the DkD planes near the secondary vertex,
iv) one track of the secondary vertex satisfying the requirements for a μ; detected by the RPC and linked to a track in the spectrometer (the iron filter removed muons with momenta less than $7\,\mathrm{GeV}/c$),
v) the momenta of the other secondary tracks greater than $3\,\mathrm{GeV}/c$,
vi) the minimum effective mass (see below) for the secondary vertex in the range 1.4–2.0 GeV/c^2,
vii) the impact parameters at the primary vertex of all secondary tracks greater than 15 μm,
viii) the effective mass of the two particles not tagged as muons inconsistent with the masses of K^0, Λ^0 or ϕ and
ix) the $K\pi\pi$ effective mass inconsistent with the D mass, so that $D \to K\pi\pi$ with π decay or punch-through should be removed (K decay does not contribute because it has the wrong charge).

If the muon had the same charge as the net charge of the tracks associated with the secondary vertex the event was called "right-sign", otherwise it was "wrong-sign". We assign pion mass to the particle which has charge equal to that of the muon and kaon mass to the other one. Assuming one missing neutrino, the minimum effective mass of the particle decaying at the secondary vertex is

$$M_{min} = (m_{vis}^2 + p_{Tvis}^2)^{1/2} + p_{Tvis},$$

where p_{Tvis} is the transverse momentum of the charged tracks, measured from the direction of the D, and m_{vis} is their effective mass. M_{min} is displayed in Fig. 1a for events with $0.846 \leq m_{K\pi} \leq 0.946\,\mathrm{GeV}/c^2$.

The effective mass spectrum for non-muon tracks from the secondary vertex is shown in Fig. 1b. The mass spectrum for "wrong-sign" events is also shown. These events do not account for the background under the K^{*0}. The difference is approximately twice the measured [12] branching fraction for $D \to K\pi\mu\nu$ where the $K\pi$ system is non-resonant, and is consistent with leakage from other decay channels (see "Backgrounds" below.)

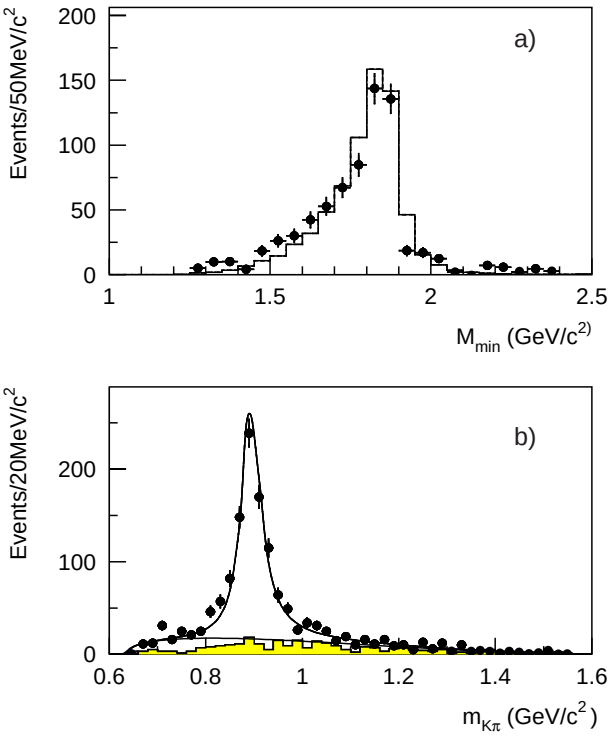

Fig. 1. a $K\pi\mu\nu_\mu$ minimum mass from background-subtracted data (*solid points*) and from simulation (*histogram*), **b** $K\pi$ invariant mass from "right-sign" data (*solid points*) and from "wrong-sign" data (*histogram*). The solid lines are fits to s- and p-wave phase-space plus relativistic p-wave Breit-Wigner

4 Backgrounds

We estimate the background remaining after event selection in two ways. In the first, the $K\pi$ mass spectrum was fitted with relativistic p-wave Breit-Wigner and s- and p-wave phase-space components, which gave $12.8 \pm 1.1\%$ for the fraction of events due to phase-space within the mass window. This fit is shown on Fig. 1b. In the second, when simulated D decays of all types were reconstructed in the usual way, we found that $14.2 \pm 1.8\%$ of the events in the mass window originated from decays other than $K^{*0}(\to K\pi)\mu\nu$, most (11.4/14.2) involving decays without K^{*0}. This is compatible with the first estimate.

5 Reconstruction of decay kinematic variables

The theoretical models [4,13] give the partial width as a function of the following complete set of kinematic variables[1] (Fig. 2):

i) θ_L; the polar angle of the muon momentum measured from the direction opposite to the D momentum in the CM frame of the virtual W,
ii) θ_V; the polar angle of the kaon momentum measured from the direction opposite to the D momentum in the CM frame of the K^*,

[1] We use decay angles as defined by [13]; their $\cos\theta_L, \phi$ correspond to $-\cos\theta, \pi - \chi$ of [4]

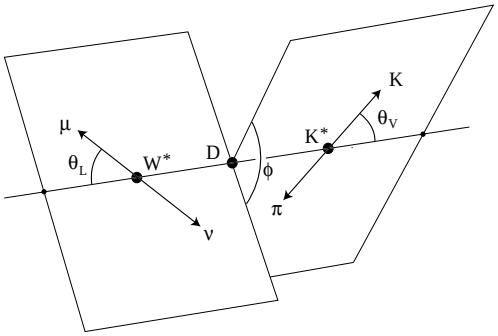

Fig. 2. The decay angles. Polar angles are defined in the CM system of the corresponding parent particle

iii) ϕ; the azimuthal angle between the decay planes of W^* and K^*, measured between the projections of the K and neutrino directions in the CM frame of the D,
iv) q^2; the square of the W^* mass and
v) $m_{K\pi}$.

We exclude $m_{K\pi}$ from the fit, since the relative values of the helicity amplitudes do not depend directly on $m_{K\pi}$, and compare data and model using the other four variables.

In order to reconstruct these kinematic variables, the momentum p_D of the D is needed. Two solutions are possible for p_D because of the unseen neutrino; we find that the two solutions reconstruct the kinematic variables in simulated events equally precisely but with a small bias of opposite sign in $\cos\theta_V$ and q^2. This is discussed further in Sect. 7. For the 20% of events where reconstruction errors make $M_{min} > M_D$, we replace M_D with ${M_{min}}^2$.

Figure 3 shows the errors found in reconstructing simulated events. Using the low-(high-)momentum solution, 47%(45%) of the events have an error in all kinematic variables of less than ±10% of their range. Such errors are small compared to the resolution needed to distinguish different values of the form factors since the expression for the decay width contains terms which vary as $\cos^2\theta_L$, $\cos^2\theta_V$, $\cos 2\phi$, q^4 or more slowly.

Figure 4 shows the acceptance projected onto each kinematic variable for simulated events. Only the distribution of $\cos\theta_L$ shows a large variation in acceptance, which is due to the loss of low-momentum muons.

6 Fitting the form-factor ratios

Ratios of form factors were determined using the maximum-likelihood method [14]. The probability distribution to be compared with data was derived from the partial decay width as given by the theoretical model [4], modulated by the acceptance as given by the simulation. This probability distribution is a function of the kinematic variables ($\cos\theta_L^i$, $\cos\theta_V^i$, ϕ^i, $(q^2)^i$) and the parameters R_V, R_2. Such

[2] This applies to the reconstruction of simulated as well as real events

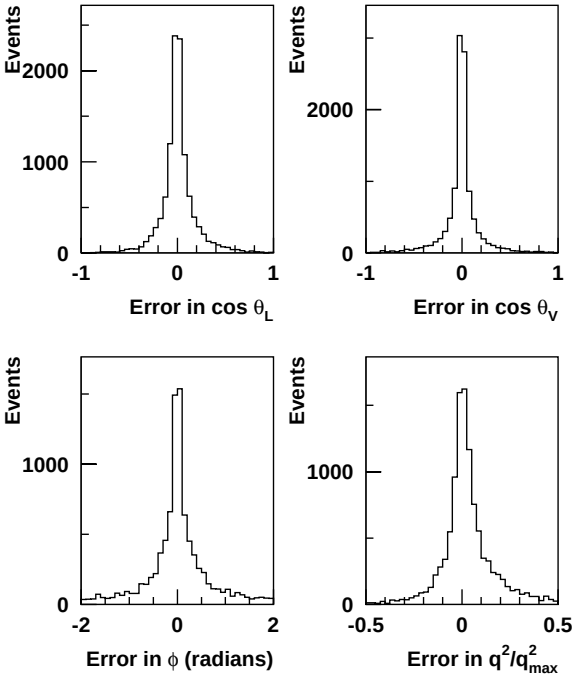

Fig. 3. Reconstruction errors in simulated events

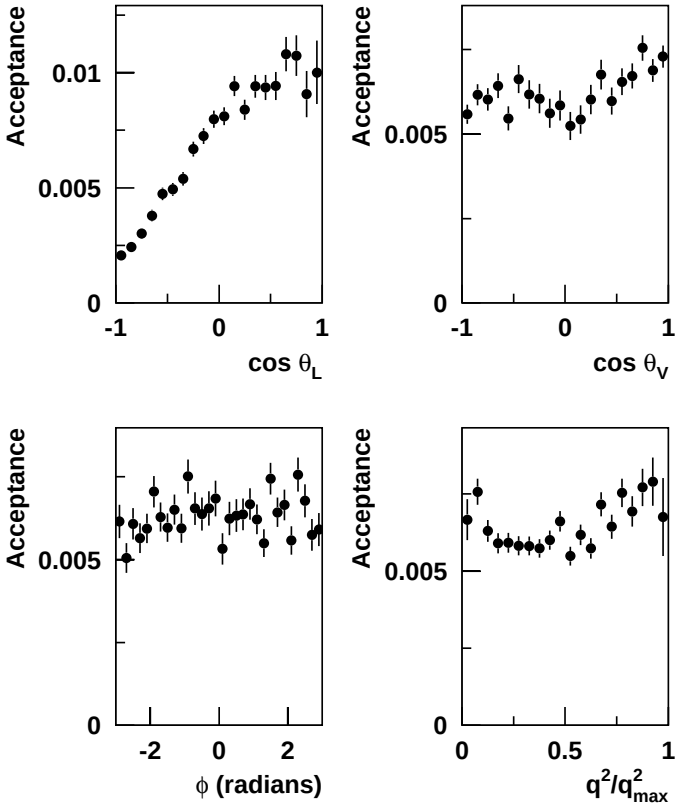

Fig. 4. Acceptance as a function of the kinematic quantities

a procedure allows for the effects of track- and vertex-finding errors, reconstruction errors and non-uniform acceptance.

The likelihood corresponding to a trial value of R_V, R_2 was calculated as follows: Each simulated event j was first pre-weighted by a function of θ_L^j and $(q^2/q^2_{max})^j$, to remove the effects of phase-space and W^* decay already present in the generation, and was then weighted using the partial decay width calculated from the model for the particular values of the kinematic variables for the event and the trial values of the parameters. (The kinematic variables were calculated from the *true* momenta for this step.)

For each data event i, its contribution to the log-likelihood was taken to be the weighted density of simulated events in its neighbourhood in the space of the kinematic variables. The neighbourhood was a hypercube with sides 1/4 the range of $\cos\theta_L^i$, $\cos\theta_V^i$ and $(q^2/q^2_{max})^i$ corresponding to about ± 2 standard deviations; for ϕ^i the neighbourhood was 1/6 in order to be sensitive to the $\cos(2\phi)$ terms. (The kinematic variables were calculated from the *reconstructed* momenta for this step.)

Contamination of the log-likelihood by background events was allowed for by estimating this contamination using events with $K\pi$ mass outside the K^{*0} region[3] and subtracting it. It is unnecessary to know the polarisation of the background, but we have to assume that events with different $K\pi$ mass are representative.

Maximising the net log-likelihood gave

$$R_V = 1.45 \pm 0.23 \quad \text{and} \quad R_2 = 1.00 \pm 0.15\ ,$$

corresponding to $\Gamma_L/\Gamma_T = 1.09 \pm 0.10$ and $\Gamma_+/\Gamma_- = 0.28 \pm 0.05$, where the errors are statistical. The magnitude of the correlation between R_V and R_2, $|\rho| < 0.03$, does not differ significantly from zero. Γ_L/Γ_T, the ratio of partial widths for longitudinal and transverse K^* polarisations, and Γ_+/Γ_-, the ratio of partial widths for positive and negative helicity, in the limit of zero lepton mass, were calculated by integrating the appropriate[4] helicity amplitudes over q^2.

In order to have an idea of the quality of the best fit, we project the data and the optimally-weighted simulated events onto the four kinematic variables (Fig. 5). The χ^2 confidence levels that the distributions for background-subtracted data and simulation are compatible are 33%, 84%, 94% and 59%.

7 Systematic errors

We have considered the following possible sources of systematic error, whose effects are summarised in Table 1.

i) *Experimental.*

[3] Background events were taken from the mass windows 0.696-0.796 GeV/c^2 and 0.996-1.096 GeV/c^2. They were weighted by 0.57 to normalise to the number of background expected in the signal region

[4] $\Gamma_L/\Gamma_T = \int_0^{q^2_{max}} pq^2 \mid H_0(q^2) \mid^2 dq^2 / \int_0^{q^2_{max}} pq^2[\mid H_+(q^2) \mid^2 + \mid H_-(q^2) \mid^2]dq^2$ and $\Gamma_+/\Gamma_- = \int_0^{q^2_{max}} pq^2 \mid H_+(q^2) \mid^2 dq^2 / \int_0^{q^2_{max}} pq^2 \mid H_-(q^2) \mid^2 dq^2$ where p is the K^* momentum in the D CM frame. Since q_{max} depends on $m_{K\pi}$, the integrals were averaged over $m_{K\pi}$

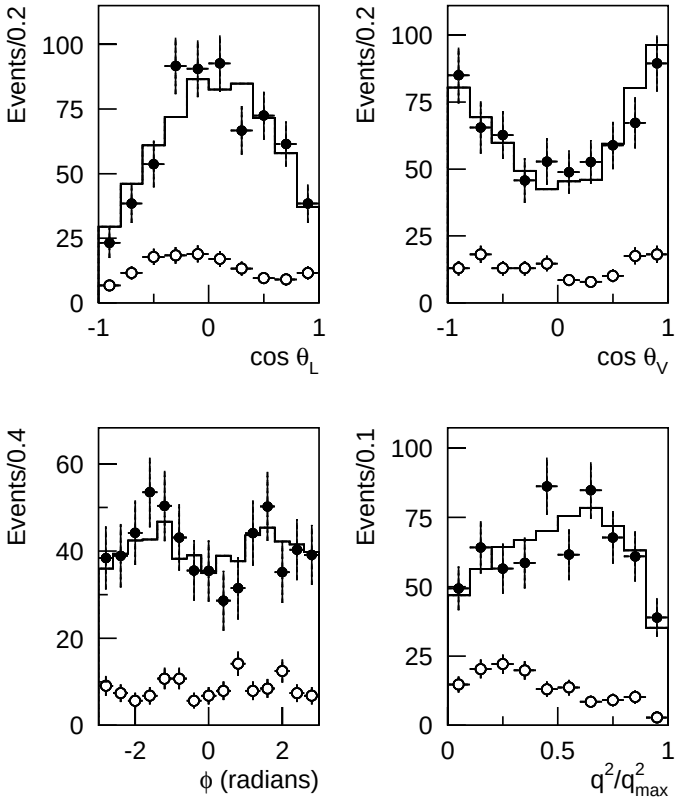

Fig. 5. Projections onto the kinematic quantities, shown for background-subtracted data (*solid circles*), for background (*open circles*) and for simulation (*histogram*)

Uncertainty in the shape of the background causes an uncertainty of 9% in the weight to be given to the events in the K^{*0} wings. In addition, there is a statistical uncertainty of 16%. By weighting the events in the K^{*0} wings accordingly, we find that the error in (R_V, R_2) is (0.02,0.01).

An independent estimate of the error due to background of the type which gives "wrong-sign" events can be obtained by using "wrong-sign" as well as "right-sign" events when making the fit. This shifted (R_V, R_2) by (0.12,0.04). There is a statistical uncertainty of ≈16% in the number of "wrong-sign" events used by the fit. The corresponding shift in (R_V, R_2) is (0.02,0.01).

There were some differences in experimental configuration and trigger for the 1992 and 1993 data samples. Fitting the data samples separately with the appropriate simulation datasets resulted in form-factor ratios consistent with (1.45,1.00) with a χ^2 probability of 13%, so at this level we see no systematic error due to the configuration.

ii) *The model of our experiment.*
The main uncertainty in acceptance comes from the loss of low-momentum muons. By comparing the momentum spectra of muons from data and simulation, we conclude that the low-momentum cutoff is known to ± 0.5 GeV/c, corresponding to $\Delta(R_V, R_2) = (0.03, 0.01)$.

Table 1. Effect of systematic errors on (R_V, R_2)

Source of error	ΔR_V	ΔR_2
Residual background	0.02	0.01
Error on p_μ cutoff	0.03	0.01
D production	0.02	0.02
Measurement errors on kinematic variables	0.00	0.01
Monte-Carlo statistics	0.06	0.02
Total	0.07	0.03

Since D^+ and D^- are produced with different longitudinal momentum distributions, they may be affected differently by this cutoff. Treating D^+ and D^- separately yields $\Delta(R_V, R_2) = (0.22, -0.21)$. The ratio of D^+ (315 events) to D^- (448 events) agrees between data and simulation within the statistical error; the effect on (R_V, R_2) is approximately $(0.02, -0.02)$.

Reconstruction of simulated events shows how well the kinematic variables of the decay are determined (Fig. 3), but it is possible that the errors in the data are different. The reconstruction program produces error estimates for the measured track and vertex quantities. The mean errors are larger for data than for simulation; in the worst case by 43% (for the dip and azimuth of the K). However, the corresponding effect on (R_V, R_2) is very small.

iii) *Monte-Carlo statistics.*
The fit used 8574 selected simulated events and 763 data. Simulated events and data occupy the same region in the space of the kinematic variables. The mean number of simulated events in the neighbourhood of each data event is then 30, but with a standard deviation of 16. When the number of simulated events was halved, (R_V, R_2) changed by (0.08,0.03), leading to an expected error of (0.06,0.02) when all simulated events are used.

iv) *Target material and trigger condition.*
The events produced on tungsten (160 out of 763) were recorded with a more severe trigger (two P_T tracks required instead of one). The results for copper and tungsten separately are compatible with the result for the whole sample within statistics.

v) *Fitting procedure and reconstruction of the D momentum.*
To see how well the fitting procedure recovers the form-factor ratios, we have weighted a subset of the simulated events with (R_V, R_2) near the measured values and treated them as data. There is no evidence for a bias in the result beyond the statistical fluctuations of 0.09 in R_V and 0.07 in R_2.

For the data, the low- and high-momentum solutions for the D momentum result in $(R_V, R_2) = (1.63,0.96)$ and (1.27,1.05), i.e. a difference of (1.6,-0.6) standard deviations, which we attribute to a statistical fluctua-

tion[5]. We see no reason to prefer one or the other and use the mean. It might be expected that the results from the two solutions would be statistically independent because when one solution is the right choice the other is wrong. However, Fig. 3 shows that the wrong choice does not give a random value for the kinematic variables. We therefore do not reduce the final statistical error.

8 Discussion

Our result is sensitive to parameters of the theoretical model other than the form-factors; here we assess that sensitivity.

We assume nearest-pole dominance [2,5,15] with masses $M_A = 2.5$, $M_V = 2.1\,\mathrm{GeV}/c^2$. Reducing the masses by $0.5\,\mathrm{GeV}/c^2$ changes (R_V, R_2) by (-0.10,-0.16). If, instead, the form-factors are taken according to a vector dominance model with dipoles (equations 35,60 of [4]), (R_V, R_2) changes by (-0.04,-0.17). In neither case does the log-likelihood change significantly.

Non-zero lepton mass has two effects. It changes the available phase-space, with the main change in the region of $q^2/q^2_{max} < 0.2$. Excluding this mass-sensitive region from the fit changes (R_V, R_2) by (-0.02,0.17), but the statistical errors increase to (0.24,0.22). Non-zero lepton mass also allows spin-flip terms in the decay rate. These involve a pseudoscalar form-factor A_0, as well as the other form-factors. We compare three values for $A_0(0)$: zero [2], $(m_D + m_{K\pi})A_1(0)/2m_{K\pi} - (m_D - m_{K\pi})A_2(0)/2m_{K\pi}$ [5] and $3A_1(0)$ [3]. The corresponding values for (R_V, R_2) are (1.48,0.96), (1.45,1.00) and (1.58,1.55). Since the log-likelihood only differs by 0.9 for the first two cases, neither can be rejected. Anyway the results are very close. The last case gives a significantly worse fit. We are, therefore, unable to distinguish between the presence of a pseudoscalar form-factor, at the level expected by [5], and its absence.

A fit to four kinematic variables is not the only possibility. To verify that the terms involving ϕ *do* improve the result, we compare the statistical errors; including ϕ reduces them slightly, from (0.28,0.16) to (0.23,0.15). (The form-factor ratios change from (1.46,0.90) to (1.45,1.00).) The log-likelihood is smaller by 10.3 when the terms involving ϕ are given a coefficient of zero so that, although the $\cos(\phi)$ and $\cos(2\phi)$ terms are not obvious in the projected distribution, we prefer the result which uses ϕ.

It has been suggested [16] that we make a fit to binned data by minimising χ^2. Although perhaps less powerful than a maximum-likelihood fit, it would give a quantitative estimate for goodness-of-fit as well as a more reliable error estimate. Four bins of $\cos\theta_L$, $\cos\theta_V$ and q^2/q^2_{max} were used. The edges were chosen, using the simulated data, to equalise the expected number of data in each bin. The fitted R_V, R_2 are (1.26,1.05) and (1.59,1.07) for the low and high D momentum solutions, yielding a mean of $(1.43 \pm 0.29, 1.06 \pm 0.17)$ compared to $(1.46 \pm 0.28, 0.90 \pm 0.16)$ from the maximum-likelihood fit with no ϕ dependence. The corresponding χ^2 probabilities are 61% and 68%. This suggests that the errors from the maximum-likelihood fit are realistic and that there is indeed a statistical fluctuation between the high- and low-momentum solutions.

[5] Our acceptance does not differ appreciably between D mesons which decay with forward neutrino and those with backward neutrino (see Sect. 5)

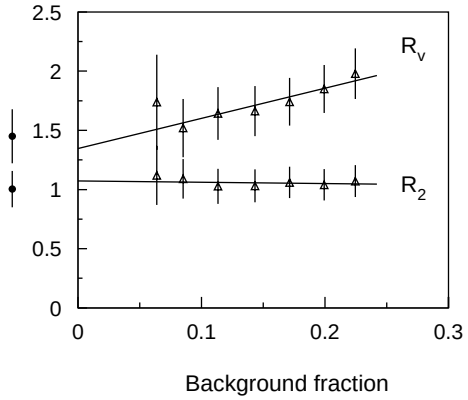

Fig. 6. Fitted R_V, R_2 as functions of the background fraction using different $K\pi$ mass windows (*open triangles*), assuming that half the background is polarised. The *closed circles* are the result of the fit using the K^{*0} wings as background. The points are not independent since they are derived from the same data sample and have many events in common

We have tried another way of dealing with the background; we make the fit using different $m_{K\pi}$ mass windows, with correspondingly different background contaminations, and extrapolate to zero contamination. We assume that half of the background is unpolarised and the rest is polarised like the signal. If the background is correctly treated, the extrapolation to zero contamination should not change (R_V, R_2). Figure 6 shows the result of these fits, with (R_V, R_2) extrapolating to (1.35±0.29, 1.07 ±0.19) at zero background. Since the extrapolation error is large and we need to make an assumption about the polarisation of the background, we do not use the value from this method in our result.

The ratio Γ_L/Γ_T can also be derived directly from the distribution of $\cos\theta_V$. Fitting the distribution obtained after subtracting events with wrong-sign muons and correcting by 1.9% for the loss of acceptance in q^2 due to the muon mass, we obtain $\Gamma_L/\Gamma_T = 0.92 \pm 0.10$(statistical) in the limit of zero lepton mass. Uncertainty in the acceptance, calculated either from simulated events weighted according to $(R_V, R_2) = (1.45,1.00)$ or from unpolarised events, causes an error in Γ_L/Γ_T of 5%. The corrections for resolution and the remaining unpolarised background each contribute 7% to Γ_L/Γ_T, with opposite signs. A similar fit made to simulated events weighted according to $(R_V, R_2) = (1.45,1.00)$ yielded $\Gamma_L/\Gamma_T = 1.06 \pm 0.04$(statistical), compared to 1.09 found directly from (R_V, R_2). This method provides a check on the polarisation which depends less on the detailed simulation of the decay.

Figure 7 and Table 2 summarise previous results together with those of the present experiment.

Table 2. Comparison of measurements of form-factor ratios

Experiment	R_V	R_2	$\Gamma_L/\Gamma_T(m_{lepton}=0)$
This expt.(μ)	$1.45 \pm 0.23 \pm 0.07$	$1.00 \pm 0.15 \pm 0.03$	$1.09 \pm 0.10 \pm 0.02$
E687 [3](μ)	$1.74 \pm 0.27 \pm 0.28$	$0.78 \pm 0.18 \pm 0.10$	$1.20 \pm 0.13 \pm 0.13$
E653 [2](μ)	$2.00^{+0.34}_{-0.32} \pm 0.16$	$0.82^{+0.22}_{-0.23} \pm 0.11$	$1.18 \pm 0.18 \pm 0.08$
E791 [17](e)	$1.84 \pm 0.11 \pm 0.08$	$0.71 \pm 0.08 \pm 0.09$	–
E691 [15](e)	$2.0 \pm 0.6 \pm 0.3$	$0.0 \pm 0.5 \pm 0.2$	$1.8^{+0.6}_{-0.4} \pm 0.3$
WA82 [18](e)	–	–	$0.6 \pm 0.3^{+0.3}_{-0.1}$

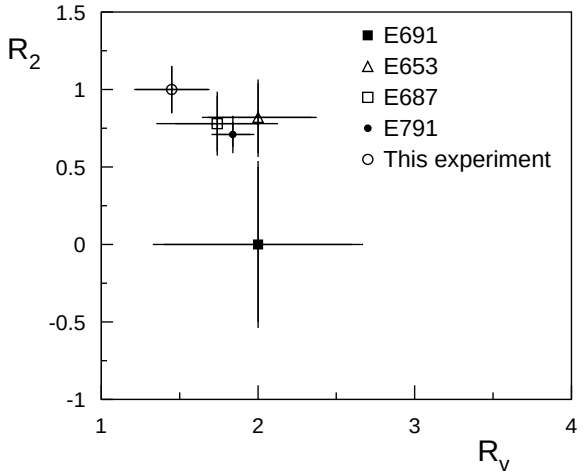

Fig. 7. Measured values for R_V, R_2. The bars represent statistical and systematic errors added in quadrature. The magnitude of the (negative) correlation coefficient is less than 0.23 in all cases

The present result is the most precise so far in the muon channel. All results are consistent with a weighted mean of (1.80,0.78), which is dominated by the E791 (electron) measurement [17].

9 Conclusion

We have used 763 $D \to K^{*0}\mu\nu_\mu$ decays to measure the D decay form-factor ratios R_V and R_2. Our result is

$$R_V = 1.45 \pm 0.23 \pm 0.07, R_2 = 1.00 \pm 0.15 \pm 0.03.$$

The corresponding ratios of partial widths, for longitudinal and transverse K^* polarisations and for positive and negative helicity, are

$$\Gamma_L/\Gamma_T = 1.09 \pm 0.10 \pm 0.02 \quad \text{and}$$
$$\Gamma_+/\Gamma_- = 0.28 \pm 0.05 \pm 0.02$$

in the limit of zero lepton mass.

Acknowledgements. We are grateful to CERN for its hospitality and to the technical support staff of Ω' and our various institutions. We acknowledge the financial support received from our national funding authorities, INFN, Italy and PPARC, UK. We thank T. del Prete and F. James for advice on statistical matters.

References

1. J.D. Richman, P.R. Burchat, Rev. Mod. Phys. **67**, 893 (1995)
2. K. Kodama et al., Phys. Lett. B **274**, 246 (1992)
3. P.L. Frabetti et al., Phys. Lett. B **307**, 262 (1993)
4. J.G. Körner, G.A. Schuler, Zeit. Phys. C **46**, 93 (1990)
5. M. Wirbel, B. Stech, M. Bauer, Zeit. Phys. C **29** 637 (1985)
6. W. Beusch et al., CERN/SPSC 77/70 (1977)
7. M. Adamovich et al., Nucl. Instrum. Methods A **379**, 252 (1996)
8. H.-U. Bengtsson, T. Sjöstrand, Comput. Phys. Commun. **46**, 43 (1987)
9. M. Bengtsson, T. Sjöstrand, Comput. Phys. Commun. **43**, (1987) 367
10. A. Fassò et al.,Proc. 4th International Conference on Calorimetry in High Energy Physics, La Biodola, Italy, 1993, Eds. A. Menzione, A. Scribano (World Scientific, Singapore, 1994) p.493
11. GEANT Detector Description and Simulation Tool, CERN Program Library Long Writeup W5013 (1994)
12. R.M.Barnett et al., Phys. Rev. D **54**, 1 (1996)
13. F.J. Gilman, R.L. Singleton, Phys. Rev. D **41**, 142 (1990)
14. D.M. Schmidt, R.J. Morrison, M.S. Witherell, Nucl. Instrum. Methods A **328**, 547 (1993)
15. J.C. Anjos et al., Phys. Rev. Lett. **65**, 2630 (1990)
16. T. del Prete, F. James, private communications
17. E.M. Aitala et al., Phys. Rev. Lett. **80**, 1393 (1998)
18. M. Adamovich et al., Phys. Lett. B **268**, 142 (1991)